J. Fluid Mech. (1995), *vol.* 289, *pp.* 129–140

An asymptotic model for the hydrodynamics of the thermal bar

By D. E. FARROW
School of Mathematics, University of East Anglia, Norwich NR4 7TJ, UK

(Received 25 May 1994 and in revised form 22 September 1994)

An asymptotic solution is found for the temperature and circulation structure for an unsteady two-dimensional model of the thermal bar phenomenon. The non-rotating case considered here is relevant to laboratory models of the thermal bar. The main implication of the asymptotic results is that the thermal bar might propagate out from the shore more slowly than predicted by a purely heat-balance-based estimate. The solution is discussed in the context of available experimental results.

1. Introduction

At the end of winter, the temperature of the water in many temperate lakes is less than 4 °C, the temperature at which water achieves its maximum density. As spring progresses and the water is warmed, the near-shore shallow waters heat more rapidly than the deeper parts. As a consequence, the 4 °C isotherm propagates out from the shore and to either side of it the horizontal pressure gradient has opposite signs. This leads to a double-cell circulation pattern with downwelling in the vicinity of the 4 °C isotherm. This isotherm is called the thermal bar and inhibits horizontal transport from the shallows to the deeper parts of the lake. A similar phenomenon occurs at the end of autumn as the lake waters are cooled towards 4 °C. The shallow waters cool more rapidly and because of the symmetry of the density relation about 4 °C, a circulation pattern similar to that which occurs during spring warming develops.

The thermal bar has been the subject of a number of field experiments, most recently by Malm *et al.* (1993). In that paper, measurements of temperature and currents during the 1991 spring thermal bar in Lake Ladoga are reported. The main results are that the isotherms are nearly vertical throughout the study region and there is a significant amount of horizontal heat transport from the warmer near-shore waters into the thermal bar region. The vertical isotherms throughout the study region are in contrast to the results of other field studies (for example, Hubbard & Spain 1973) which show a stably stratified region on the warmer near-shore side of the thermal bar. The vertical isotherms observed by Malm *et al.* are due to the significant amount of wind-induced vertical mixing. Malm *et al.* also observed a complex, largely wind driven, circulation pattern.

Experimental studies of the thermal bar have been carried out by Elliott & Elliott (1969, 1970) and Kreyman (1989). Those experiments were able to reproduce in the laboratory many of the features of the thermal bar observed in the field. In those experiments, water at less than 4 °C contained in a shallow triangular tank was heated from above. In the experiments of Elliott & Elliott, the heating was via infra red lamps which meant that most of the heat input occurs in the top 1 or 2 cm of the 13 cm deep tank. This led to a strongly stratified warm region in the shallow end of the tank behind the thermal bar and a vertically well-mixed cold region ahead of the thermal bar. This

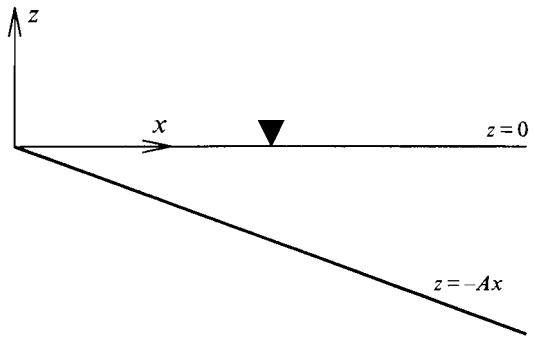

FIGURE 1. Schematic of the flow domain and the coordinate system with the origin at the tip of the wedge. The solid triangle indicates the position of the fluid surface.

is very similar to the structure observed in Lake Superior by Hubbard & Spain (1973). The surface heating in the experiments of Kreyman (1989) was via lamps with most of their heat in the visible spectrum. This meant that the heat penetrated deeper into the water and led to a weaker stratification in the shallows than that observed by Elliott & Elliott.

Most theoretical studies of the thermal bar have concentrated on modelling the heat budget associated with the propagation of the thermal bar. Elliott & Elliott (1970) developed a two-dimensional model which ignored the horizontal transport of heat. They were able to obtain an expression for the position of the thermal bar as a function of time. Zilitinkevich, Kreiman & Terzhevik (1992) describe a more complex model that allows for the horizontal transport of heat from the warm shallow regions into the vicinity of the thermal bar thereby increasing its propagation speed. Huang (1972) derived an asymptotic solution (based on small Rossby number) for the steady-state temperature and circulation pattern of an idealized model of Lake Michigan. Elliott (1970) developed a model for the circulation associated with the thermal bar by assuming a balance between vertical shear and the horizontal pressure gradient. In that model, the flow was driven by an unsteady temperature field derived by a one-dimensional (in the vertical) diffusion equation with a surface heat flux. Elliott found good agreement between his results and the experimental results of Elliott & Elliott (1969, 1970).

Bennett (1971) carried out a numerical investigation of the thermal bar. Bennett's model was fully three-dimensional and included rotational effects. The results predicted that motion would be largely confined to the warm near-shore region and that the flow would be in geostrophic balance. He also concluded that horizontal heat transport could be important in the shallows but that there appeared to be no significant heat transport into the thermal bar region.

In the current work, an asymptotic solution based on the smallness of the bottom slope is found for an unsteady non-rotating two-dimensional model of the thermal bar phenomenon. The observations of Malm *et al.* (1993) show that the thermal bar moves into deep water more rapidly than a viscous balance can occur; thus unsteady inertial effects could be important in determining the overall circulation pattern. The results of the asymptotic analysis will be discussed in the context of available experimental results.

2. Model formulation

The spring thermal bar is modelled by the unsteady two-dimensional natural convection of an incompressible fluid contained in the non-rotating triangular domain lying between the lines $z = 0$ and $z = -Ax$ where A is the bottom slope, in the (x, z)-plane. A schematic of the flow domain and coordinate system is shown in figure 1. Density differences associated with the thermal bar are generally quite small so the Boussinesq approximation is appropriate. The equations governing the flow and temperature are therefore

$$\frac{\partial u}{\partial t}+u\frac{\partial u}{\partial x}+w\frac{\partial u}{\partial z}=-\frac{1}{\rho_0}\frac{\partial p}{\partial x}+\nu\nabla^2 u, \tag{1}$$

$$\frac{\partial w}{\partial t}+u\frac{\partial w}{\partial x}+w\frac{\partial w}{\partial z}=-\frac{1}{\rho_0}\frac{\partial p}{\partial z}+\nu\nabla^2 w-\frac{g(\rho-\rho_0)}{\rho_0}, \tag{2}$$

$$\frac{\partial T}{\partial t}+u\frac{\partial T}{\partial x}+w\frac{\partial T}{\partial z}=\kappa\nabla^2 T+Q, \tag{3}$$

$$\frac{\partial u}{\partial x}+\frac{\partial w}{\partial z}=0, \tag{4}$$

where u and w are the horizontal and vertical velocities respectively, T is the temperature, p is the pressure perturbation, ρ is the density, ρ_0 is the reference density, ν is the kinematic viscosity, κ is the thermal diffusivity and g is the acceleration due to gravity. The model is driven by the heat source term Q in (3). The precise form of Q is specified later in this section.

For the thermal bar, the nonlinear relationship between ρ and T is of particular importance. In this work, this relationship is assumed to take the form

$$\rho-\rho_0=\rho_0\frac{a_1\Delta T-a_2\Delta T^2}{1+b\Delta T}, \tag{5}$$

where $\Delta T = T-T_0$, $\rho_0 = \rho(T_0)$ and a_1, a_2 and b are all constants dependent on T_0. The above form for ρ is obtained by truncating the representation found in Gebhart *et al.* (1988, Appendix F). The truncated form (5) is quite accurate over the range of temperatures associated with the thermal bar and captures the linear relationship for large and small T as well as the quadratic relationship near the density maximum. Table 1 gives values of the constants in (5) for various values of T_0. The temperature/density relationship (5) is a little more complicated than the usual quadratic form associated with modelling water close to its density maximum. The more complicated form is introduced here to ensure that fluid velocities vanish as $x \to 0$.

The flow in this model is driven by a flux of heat into the fluid represented by the heat source term Q on the right-hand side of (3). In this model, it is assumed that a spatially uniform surface heat flux of I_0 W m^{-2} is distributed uniformly over the local depth. The assumption of a vertically uniform source of heat is a considerable simplification of the heat input and output mechanisms operant in a real lake. In particular, most of the heating occurs at or near the surface. The heating in a real lake also varies spatially and with time. A more sophisticated model for the thermal forcing would considerably complicate the subsequent analysis as well as involve extra parameters that would need to be specified. Also, the interest in this paper is in the bulk

T_0 (°C)	ρ_0 (kg m^{-3})	a_1 (°C^{-1})	a_2 (°C^{-2})	b (°C^{-1})
0	999.8396	6.836×10^{-5}	8.396×10^{-6}	1.145×10^{-2}
1	999.8986	5.031×10^{-5}	8.301×10^{-6}	1.132×10^{-2}
2	999.9400	3.286×10^{-5}	8.207×10^{-6}	1.119×10^{-2}
3	999.9643	1.599×10^{-5}	8.116×10^{-6}	1.107×10^{-2}

TABLE 1. Values for the constants ρ_0, a_1, a_2 and b in (5) for various values of the reference temperature T_0.

behaviour of the thermal bar rather than the details of the thermal forcing. It is for these reasons that this work is restricted to vertically uniform heating. The assumptions outlined above yield an expression for Q dependent only on x:

$$Q = I_0/(\rho_0 C_p A x) \text{ °C s}^{-1}, \tag{6}$$

where C_p is the specific heat of water. The x-dependence in (6) will give rise to horizontal gradients in temperature that will subsequently drive a flow.

To complete the model, it only remains to specify the boundary and initial conditions. The surface is supposed to be stress free and not deformed, which leads to the boundary conditions

$$\frac{\partial u}{\partial z} = w = 0 \quad \text{on} \quad z = 0. \tag{7}$$

The bottom boundary is supposed to be rigid and non-slip and so

$$u = w = 0 \quad \text{on} \quad z = -Ax. \tag{8}$$

It is assumed that all the heat input is included in the heat source term Q. This means that there are no heat fluxes through either the upper or lower boundaries, thus

$$\frac{\partial T}{\partial z} = 0 \quad \text{on} \quad z = 0, \tag{9}$$

$$A\frac{\partial T}{\partial x} + \frac{\partial T}{\partial z} = 0 \quad \text{on} \quad z = -Ax. \tag{10}$$

The model is started from rest with the fluid at a uniform temperature T_0, so the initial conditions are

$$u = w = 0, \quad T = T_0 \quad \text{at} \quad t = 0. \tag{11}$$

Finally, as $x \to \infty$, the dependent variables relax to the initial conditions.

3. Asymptotic solution

Unfortunately the model outlined in the previous section does not admit a general analytic solution. In this section, an asymptotic solution as the bottom slope $A \to 0$ is obtained. To this end, the system of equations defining the model is first non-dimensionalized.

Neither the geometry of the flow domain nor the form of the forcing provide any obvious time or length scales. However, scales can be derived in the following way. Balancing the unsteady and source terms in (3) yields a scale for $T - T_0$:

$$T - T_0 \sim I_0 t/(\rho_0 C_p A x). \tag{12}$$

The horizontal position at which $T = T_m$ (where T_m is a temperature scale) is given by

$$x_m \sim I_0 t/((T_m - T_0)\rho_0 C_p A) \tag{13}$$

where the local depth will be $h_m = Ax_m$. Viscous effects will be felt over the depth h_m in a time scale $\tau = h_m^2/\nu$. Identifying t with τ yields length and time scales for this model:

$$x \sim l = \nu(T_m - T_0)\rho_0 C_p/(AI_0), \tag{14}$$

$$z \sim h = \nu(T_m - T_0)\rho_0 C_p/I_0, \tag{15}$$

$$t \sim \tau = \nu((T_m - T_0)\rho_0 C_p/I_0)^2. \tag{16}$$

The temperature T_m needs to be specified and the obvious physical choice is the temperature at which the water density is at its maximum. However, for algebraic convenience, T_m is chosen so that the numerator of (5) is at its maximum, that is $T_m - T_0 = a_1/2a_2$. In practice, T_m is very close to the maximum density temperature. The time scale (16) can be interpreted as the time after which viscous effects cease to be felt over the entire water depth at the thermal bar.

Balancing the buoyancy and pressure gradient terms in (2) yields a scale for the pressure perturbation $p \sim gh\Delta\rho_0$ where $\Delta\rho_0 = \rho_0 a_1^2/(2a_2)$ and h is given by (15). Substituting this scale into (1) and balancing the viscous and pressure gradient terms yields a scale for the horizontal velocity:

$$u \sim U = AGrh/\tau, \tag{17}$$

where the Grashof number Gr is given by

$$Gr = g\Delta\rho_0 h^3/\rho_0 \nu^2. \tag{18}$$

Finally, the continuity equation (4) yields a scale for $w \sim AU$.

The scales outlined above can be used to non-dimensionalize the model equations of §2. The non-dimensional equations are still intractable but an asymptotic solution can be found as $A \to 0$ (see Cormack, Leal & Imberger 1974; Farrow & Patterson 1993). In the limit as $A \to 0$, the model equations become

$$u_t^{(0)} = -p_x^{(0)} + u_{zz}^{(0)}, \tag{19}$$

$$0 = -p_z^{(0)} - \frac{T^{(0)} - T^{(0)^2}/2}{1 + \gamma T^{(0)}}, \tag{20}$$

$$u_x^{(0)} + w_z^{(0)} = 0, \tag{21}$$

$$T_t^{(0)} = T_{zz}^{(0)}/\sigma + 1/x, \tag{22}$$

where $\gamma = ba_1/2a_2 (\approx 4.66 \times 10^{-2}$ for $T_0 = 0$ °C), $\sigma = \nu/\kappa$, $(\cdot)^{(0)}$ indicates the $O(A^0)$ solution and all variables are now non-dimensional. The boundary and initial conditions become

$$T_z^{(0)} = u_z^{(0)} = w^{(0)} = 0 \quad \text{on} \quad z = 0, \tag{23}$$

$$T_z^{(0)} = u^{(0)} = w^{(0)} = 0 \quad \text{on} \quad z = -x, \tag{24}$$

$$T^{(0)} = u^{(0)} = w^{(0)} = 0 \quad \text{at} \quad t = 0. \tag{25}$$

Thus, at $O(A^0)$, the flow is governed by the linearized shallow-water equations. Also, the asymptotics have eliminated all horizontal processes which are second-order effects. The horizontal coordinate x now becomes a parameter specifying the local conditions.

The $O(A^0)$ temperature $T^{(0)}$ is easily found and is given by

$$T^{(0)} = t/x \tag{26}$$

and represents an ever increasing horizontal temperature gradient. The $O(A^0)$ horizontal velocity can be found using Laplace transform methods. The details are contained in the Appendix and only the solution is presented here:

$$u^{(0)} = \sum_{n=1}^{\infty} g_n(x,z) f_n(x,t), \tag{27}$$

where

$$g_n(x,z) = -(\cos\beta_n + (\cos\beta_n - 1)/\beta_n^2 - \tfrac{1}{2})(\beta_n \cos(\beta_n z/x) - \sin\beta_n)/\beta_n^6 \sin\beta_n, \tag{28}$$

$$\begin{aligned} f_n(x,t) = \Bigg[& \int_0^{(\beta_n/x)^2 t} \frac{\mathrm{e}^{-\tau}}{(\beta_n/x)^2 (x+\gamma\tau)/\gamma - \tau} \mathrm{d}\tau\, \beta_n^4 (1+2\gamma)(\gamma x - \beta_n^2)(x+\gamma t) \\ & + (\exp(-(\beta_n/x)^2 t) - 1)\gamma x^2(\gamma^3 x t + \gamma^2 x^2 + 2\beta_n^4 \gamma + \beta_n^4) \\ & + \exp(-(\beta_n/x)^2 t)\gamma^2 x \beta_n^4 t(1+2\gamma) + \gamma^3 x t \beta_n^2 (x+\gamma t) \Bigg] \Big/ \gamma^4 (x+\gamma t), \end{aligned} \tag{29}$$

and β_n are the positive roots of $\sin\beta_n = \beta_n \cos\beta_n$.

4. Discussion

4.1. *Temperature structure*

The $O(A^0)$ temperature $T^{(0)} = t/x$ is nothing more than then non-dimensional form of (12) and reflects a balance between the source term Q and the rate of increase of temperature. The lack of any dependence of Q on z and the insulated boundary conditions mean that diffusion plays no role in determining $T^{(0)}$. The solution represents an ever increasing horizontal temperature (and thus density) gradient that is greater towards the shore $x = 0$. The non-dimensional temperature at which the density is maximum depends weakly on γ which in turn is a function of T_0. For $T_0 = 0$ °C, the density maximum occurs at $T^{(0)} \approx 0.98$, thus the position of the thermal bar is given by

$$l_T = 1.023t. \tag{30}$$

This is the non-dimensional equivalent of Elliott & Elliott's (1970) model and its evolution with time is shown as the heavy solid line in figure 2. The volume-averaged temperature behind the thermal bar is $\bar{T}_l \approx 1.96$, a constant. In the model described by Zilitinkevich *et al.* (1992) there is a horizontal heat flux into the thermal bar region from the near-shore waters which leads to $\bar{T}_l$ decreasing with time. That heat flux also causes the thermal bar to advance more rapidly in their model. In the asymptotic model of this paper, horizontal heat transfer is neglected, thus $\bar{T}_l$ is constant with time.

4.2. *Velocity structure*

A summary of the overall evolution of the flow is presented in figure 2 where contours of the surface velocity $u^{(0)}|_{z=0}$ are shown in the (t,x)-plane. The thin solid line is the zero contour and represents the point on the surface where downwelling occurs. At all times and all positions, the direction of the surface velocity is towards the downwelling front. Note that for $t > 1$, the downwelling front noticeably lags the thermal bar; the thermal bar is moving out from the shore more rapidly than the downwelling front. For $x > 1$, the main balance is between inertia and the horizontal pressure gradient. The lag is due to the time taken for the change in sign of the horizontal pressure gradient associated with the passing of the thermal bar to decelerate the existing flow. For $x < 1$, the main balance is between vertical shear and the pressure gradient; thus

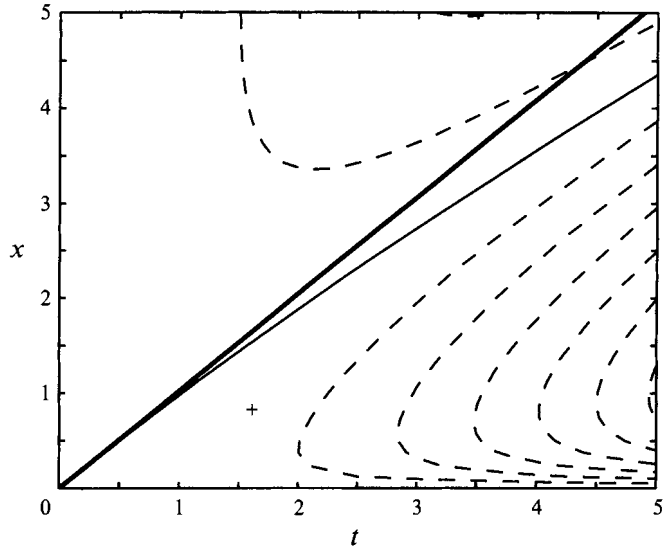

FIGURE 2. Contours of the surface velocity $u^{(0)}|_{z=0}$ in the (t, x)-plane. The contour interval is 0.05 and the solid contour is the zero contour. The heavy solid line indicates the position of the thermal bar and the + and − symbols indicate the sign of the surface velocity.

the flow there reverses as soon as the pressure gradient changes sign. If vertical shear is ignored in (19) then $u^{(0)}$ is given by

$$u^{(0)} = u_i^{(0)} = -\frac{z+x/2}{4\gamma^3 x^2(x+\gamma t)}[2x^2(2\gamma+1)(x+\gamma t)\log(1+\gamma t/x) - \gamma t(\gamma t(x+\gamma t)+2x^2(1+2\gamma))]. \quad (31)$$

This is simply a linear velocity profile and does not satisfy the stress-free and no-slip boundary conditions. Also, $u_i^{(0)}$ is unbounded as $x \to 0$. It can be shown that $u_i^{(0)}|_{z=0} = 0$ when $x/t \approx 0.683$. Thus a purely inertial model of the flow would predict that the propagation speed of the downwelling front is approximately 33 % less than that of the thermal bar. The slope of the zero contour in figure 2 for large x is close to the value of 0.683 predicted by an inertial balance.

The internal structure of the flow as it evolves is shown in figure 3 where streamlines at various times are plotted. In each plot, the dashed line indicates the position of the thermal bar at that time. At each time there is a dividing streamline that intersects the surface $z = 0$ at the downwelling front. Ahead of the dividing streamline the circulation is anticlockwise, while behind it the circulation is clockwise. In figure 3(*a*), the downwelling front is still in the viscous region. Thus the dividing streamline is close to vertical and there is a relatively weak circulation near the shore. At the later time of $t = 3$ (figure 3*b*), the downwelling front significantly lags the thermal bar and the dividing streamline now has a significant slope towards the shore. Note that the change in sign in the pressure gradient occurs simultaneously over the entire depth and so the viscous-dominated flow near the rigid bottom boundary is the first to reverse. This means that the dividing streamline must attach to $z = -x$ at $x \approx 1.023t$. As time increases (figure 3*c*) and the flow in the vicinity of the thermal bar becomes increasingly dominated by inertia, the average slope of the dividing streamline decreases (from the vertical) eventually approaching the value of approximately -3.01 predicted by the inertial balance described above.

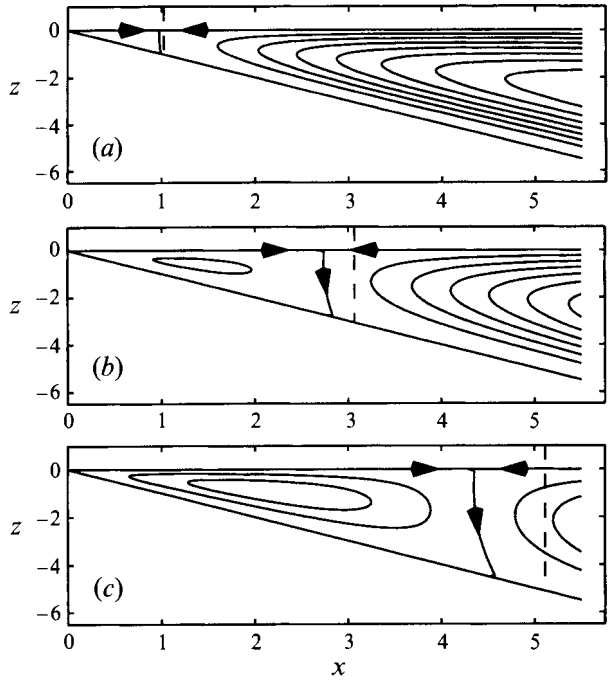

FIGURE 3. Streamline plots at various times (*a*) $t = 1$, (*b*) $t = 3$ and (*c*) $t = 5$. In each plot, the vertical dashed line indicates the position of the density maximum and the arrows indicate the direction of the flow. The contour interval in each case is (*a*) 0.005, (*b*) 0.025 and (*c*) 0.05.

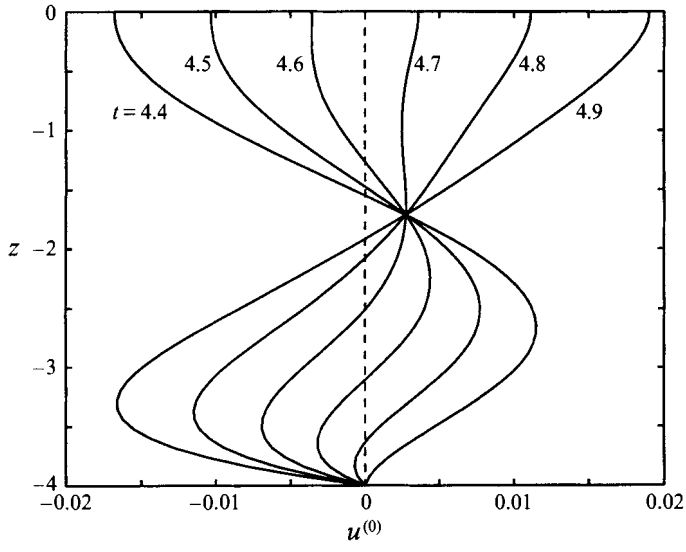

FIGURE 4. Velocity profiles at various times at $x = 4$ as the downwelling front passes. At $t = 4.5$ and $t = 4.6$, a three-layer velocity structure is evident.

The tilting over of the dividing streamline is reflected in the complex structure of the velocity reversal. A number of velocity profiles at $x = 4$ as the downwelling front passes are shown in figure 4. At $x = 4$ the pressure gradient reverses at $t \approx 3.9$. The surface velocity does not change sign until $t \approx 4.65$ and at $t = 4.5$ and $t = 4.6$, a three-layer

velocity structure is evident. It has already been noted that the pressure gradient reversal occurs over the entire depth at the same time so the viscous-dominated flow next to the rigid bottom boundary is the first to reverse. As time increases ($t = 4.7$–4.9), the reversed flow increases in strength approximately linearly in time reflecting the largely inertial balance that applies at $x = 4$. More precisely, the background pressure gradient is changing with time so the magnitude of the velocities in figure 4 include nonlinear terms. However, over the relatively short range of times presented in figure 4, the magnitude of the forcing has not changed much and the linear-in-t dependence is more obvious.

4.3. *Relation to experiments*

The most recent experimental results pertaining to the thermal bar are reported by Kreyman (1989) and Zilitinkevich *et al.* (1992). In terms of the dimensionless variables of this paper the experimental tank has a non-dimensional length in the range $l = 2$–3.7. This suggests that approximately half of the flow will be in the viscous regime described above. The maximum fluid velocity observed in those experiments was approximately 10^{-4} m s^{-1}. Estimates of the maximum velocity from the asymptotic results range from 3×10^{-4} to 8×10^{-4} m s^{-1} for the various experiments reported. This is a considerable over-estimate which could be due to a number of factors. The predicted maximum velocities all occur in the warm region near the shore where in the experimental results there is a significant amount of stable temperature stratification. It was noted by Farrow & Patterson (1994) that if some of the available thermal energy is used to create a stable stratification then there is less energy available to drive a flow. They reported that velocities could be an order of magnitude less in this case. Also, horizontal diffusion and differential heat loss through the surface would lessen the horizontal pressure gradient and lead to lower velocities than those predicted by the asymptotic results.

In all the experiments reported by Kreyman (1989), the thermal bar progressed more slowly than the simple heat budget estimate of $u_f = I_0/\Delta T_0 \rho_0 C_p A$. For all experiments, the measured speed was between 7% and 36% less than the theoretical estimate. The value of 36% is somewhat anomalous and is based on scanty data; the next smallest difference is 19%. This difference in propagation speed is of the same order of magnitude as the difference between the propagation speeds of the thermal bar and the downwelling front in figure 2. Approximately half of the flow occurs in the inertia-dominated regime so the discrepancy between the theoretical estimate and the experimental results could be due to the advection of cooler water ahead of the downwelling front towards $x = 0$. This would be a second-order effect in the current asymptotic solution. The complete non-dimensional temperature equation is

$$\overbrace{T_t}^{O(A^0)} + A^2 Gr(uT_x + wT_z) = (A^2 T_{xx} + \overbrace{T_{zz}}^{O(A^0)})/\sigma + \overbrace{Q}^{O(A^0)}, \tag{32}$$

where it has been made explicit which terms are included in the $O(A^0)$ solution. Using the $O(A^0)$ solution and the parameters of Kreyman (1989) to estimate the various terms in (32) at $(x, t) = (1, 1)$ (i.e. halfway along the tank) yields

$$T_t \approx 1, \quad A^2 GruT_x \approx 0.2, \quad A^2 T_{xx}/\sigma \approx 0.002, \quad Q \approx 1. \tag{33}$$

The other terms in (32) are identically zero according to the $O(A^0)$ solution. The above estimates suggest that horizontal advection could have an effect on the heat budget and this could lead to the difference between the predicted and measured propagation speeds of the thermal bar.

A further feature of the asymptotic results is the tilting over of the dividing streamline as the thermal bar moves from the viscous regime in the shallows to the inertial regime in the deeper waters. In the limit as the flow is dominated by an inertia and pressure gradient balance, the dividing streamline would be at an angle of approximately 19° to the horizontal. This could explain the change from symmetric to non-symmetric traces on either side of the thermal bar reported by Zilitinkevich *et al.* (1992). In the viscous regime, the velocity is essentially modulated by the sign and magnitude of the pressure gradient, whilst in the deeper waters, the inertia of the existing flow plays a role in the dynamics. In particular it leads to a three-layer velocity structure as the thermal bar passes. Another possible explanation is the presence of a warm surface jet emanating from the shallows similar to that observed by Ivey & Hamblin (1989).

Many of the above remarks carry over to the experiments reported by Elliott & Elliott (1969, 1970). The experimental tank used by Elliott & Elliott was approximately the same size as that used by Kreyman (1988) and the magnitude of the surface heating was similar. The main differences between the models was that Elliott & Elliott had a rigid lid at the surface and infra-red lamps were used as heat sources. The rigid lid meant that the fluid velocity, rather than the stress, was zero at the surface. The infra-red lamps led to most of the heat being absorbed in the upper 1 or 2 cm of the water rather than more evenly over the depth of the tank.

4.4. *Validity of asymptotic solution*

Since $T^{(0)}$ is singular at $x = 0$ (and hence the horizontal gradient is also singular), the range of validity of the asymptotic solution needs to be addressed. Also, the model of this paper has no steady state as heat is continuously added but none is permitted to escape. This means that the dependent variables are unbounded as $t \to \infty$.

The asymptotic solution found in §3 can be expected to yield reasonable results as long as the terms not included in the $O(A^0)$ equations are dominated by those that are included. Using $T^{(0)}$ to estimate the size of the various terms in the full heat equation (32), the horizontal conduction term $A^2 T_{xx}/\sigma \propto x^{-3}$. The terms included in the $O(A^0)$ equation are all proportional to x^{-1}. This means that no matter how small A is, there will always be some region near $x = 0$ where the neglected conduction term is larger than those terms that are not neglected. An estimate of the size of this region can be obtained by demanding that $T_t > A^2 T_{xx}/\sigma$. This yields a criterion for validity $x > A(2t/\sigma)^{1/2}$. The effect of this failure is relatively minor. In practice, it means that the horizontal gradients near $x = 0$ will be over-estimated due to horizontal conduction being neglected. This in turn means that velocities there will be over-estimated.

It can be shown that the surface velocity $u^{(0)}|_{z=0}$ has the following properties far from the thermal bar (so that the density/temperature relationship is linear):

$$u^{(0)}|_{z=0} \to \begin{cases} -t^2/(4x), & x > 1, \quad \text{inertial balance} \\ tx/(96\gamma), & x < 1, \quad \text{viscous balance.} \end{cases}$$

In the inertial regime, the condition that $T_t > A^2 Gru T_x$ yields a time limit on the range of validity of the asymptotic solution

$$t < t_i = \left(\frac{4x^2}{A^2 Gr}\right)^{1/3}$$

while in the viscous regime, the same condition yields

$$t < t_v = \left(\frac{96\gamma}{A^2 Gr}\right)^{1/2}.$$

For the experiments of Kreyman (1989), $A = 0.1$ and $\sigma \approx 10$. A representative value for the Grashof number is $Gr = 10^4$. The non-dimensional length of the experimental tank is $l \approx 3$. Substitution yields $t_i \approx 0.71$ and $t_v \approx 0.14$. The time limit in the viscous regime is likely to be very conservative as it is based on much larger temperature gradients than are achieved in the laboratory. The values of t_i and t_v above indicate that the asymptotic results are appropriate for the initial stage of the experiments but for later times neglected effects, notably advection, affect the dynamics. It is not clear how the breakdown of the asymptotic results will appear. It could be, for example, via the formation of a warm surface jet similar to that observed by Ivey & Hamblin (1989).

5. Concluding remarks

The main conclusion to be drawn from the asymptotic results of this paper is that the inertia of the circulation associated with the thermal bar could reduce its propagation speed. The increasing importance of inertial effects as the thermal bar moves into deeper waters could also account for some of the experimental observations such as the transition to non-symmetric velocity profiles on either side of the thermal bar.

There are number of generalizations that could be made to improve the model of §2. Uppermost is the inclusion of vertically non-uniform heating to more accurately represent the heating operant in the field and laboratory experiments. The results of Zilitinkevich *et al.* (1992) show that the horizontal heat transport is important for the propagation of the thermal bar. The asymptotic model of this paper neglects this effect and thus does not provide any insight into the heat transport process. For many lakes, Coriolis effects can also be significant. It is not clear how any of these effects can be included without considerably complicating the analysis of this paper.

Further work should also include numerical simulations which would allow examination of the fully nonlinear problem. Even for small bottom slopes, if Gr is sufficiently large, the advection of heat and momentum is important in the dynamics.

The author gratefully acknowledges useful remarks made by J. Johnson, S. Brown and the anonymous reviewers on earlier versions of this paper.

Appendix

The method for finding the $O(A^0)$ velocity solution proceeds as follows. The pressure is eliminated from (19) and (20) by cross-differentiation. Introducing a stream function ψ with $u^{(0)} = -\psi_z$ and $w^{(0)} = \psi_x$ yields

$$\frac{\partial^3 \psi}{\partial t \, \partial z^2} = \frac{\partial^4 \psi}{\partial z^4} + \frac{\partial}{\partial x}\left[\frac{T^{(0)} - T^{(0)^2}/2}{1 + \gamma T^{(0)}}\right]. \tag{A 1}$$

The solution is found by first finding the solution to (A 1) with the forcing term on the right-hand side replaced by $\delta(t)$, the Dirac delta function. The solution that satisfies boundary conditions (23)–(25) is

$$\psi_0 = 2x \sum_{n=1}^{\infty} \frac{\exp\left(-(\beta_n/x)^2 t\right)}{\beta_n^2 \sin \beta_n} (\cos \beta_n + (\cos \beta_n - 1)/\beta_n^2 - \tfrac{1}{2})(x \sin(\beta_n z/x) - z \sin \beta_n), \tag{A 2}$$

where β_n are the positive roots of the equation $\sin\beta_n = \beta_n \cos\beta_n$. After substitution for $T^{(0)}$ and differentiation, the solution to (A 1) is given by

$$\psi = \frac{1}{2x^2}\int_0^t \psi_0(t-\tau)\frac{\gamma\tau^2+2\tau x-2x^2}{(x+\gamma\tau)^2}\tau\,\mathrm{d}\tau. \tag{A 3}$$

The expression for $u^{(0)}$ given by (27) follows.

REFERENCES

BENNETT, J. R. 1971 Thermally driven lake currents during the spring and fall transition periods. In *Proc. 14th Conf. Great Lakes Res.* pp. 535–544. Intl Assoc. Great Lakes Res.

CORMACK, D. E., LEAL, L. G. & IMBERGER, J. 1974 Natural convection in shallow cavity with differentially heated end walls. Part 1. Asymptotic theory. *J. Fluid Mech.* **65**, 209–229.

ELLIOTT, G. H. 1970 A mathematical study of the thermal bar. In *Proc. 13th Conf. Great Lakes Res.* pp. 545–554. Intl Assoc. Great Lakes, Res.

ELLIOTT, G. H. & ELLIOTT, J. A. 1969 Small-scale model of the 'thermal bar'. In *Proc. 12th Conf. Great Lakes Res.* pp. 553–557. Intl Assoc. Great Lakes Res.

ELLIOTT, G. H. & ELLIOTT, J. A. 1970 Laboratory studies on the thermal bar. In *Proc. 13th Conf. Great Lakes Res.* pp. 413–418. Intl Assoc. Great Lakes Res.

FARROW, D. E. & PATTERSON, J. C. 1993 On the response of a reservoir sidearm to diurnal heating and cooling. *J. Fluid Mech.* **246**, 143–161.

FARROW, D. E. & PATTERSON, J. C. 1994 The daytime circulation and temperature structure in a reservoir sidearm. *Intl J. Heat Mass Transfer* **37**, 1957–1968.

GEBHART, B., JALURIA, Y., MAHAJAN, R. L. & SAMMAKIA, B. 1988 *Buoyancy-Induced Flows and Transport.* Hemisphere.

HUANG, J. C. K. 1972 The thermal bar. *Geophys. Fluid Dyn.* **3**, 1–28.

HUBBARD, D. W. & SPAIN, J. S. 1973 The structure of the early spring thermal bar in Lake Superior. In *Proc. 16th Conf. Great Lakes Res.* pp. 735–742. Intl Assoc. Great Lakes Res.

IVEY, G. W. & HAMBLIN, P. F. 1989 Convection near the temperature of maximum density for high Rayleigh number, low aspect ratio, rectangular cavities. *Trans. ASME J. Heat Transfer* **111**, 100–105.

KREYMAN, K. D. 1989 Thermal bar based on laboratory experiments. *Oceanology* **29**, 695–697.

MALM, J., GRAHN, L., MIRONOV, D. & TERZHEVIK, A. 1993 Field investigation of the thermal bar in Lake Ladoga, spring 1991. *Nordic Hydrology* **24**, 339–358.

ZILITINKEVICH, S. S., KREIMAN, K. D. & TERZHEVIK, A. YU. 1992 The thermal bar. *J. Fluid Mech.* **236**, 27–42.